GIS Odyssey Journal

2026 • Volume 6 • Number 1

https://doi.org/10.57599/gisoj.2026.6.1.79

Ayehu Fekadu[1], Belew Bekele[2]

ASSESSING THE EFFECTS OF TEMPERATURE CHANGE ON HUMAN THERMAL COMFORT UNDER INTENSIFYING LAND COVER CHANGE IN ETHIOPIA (1984–2023)

Abstract: Rising temperatures have aggravated heat stress in many tropical countries, driven by the combined effects of land cover dynamics and climate variability. However, the impacts of land use and land cover change (LULC) on thermal comfort have not been sufficiently evaluated, predominantly in many African countries. Thus, this study assesses heat stress in Ethiopia (1984–2023) using Adjusted Wet-Bulb Globe Temperature (WBGT) and Discomfort Index (DI) assessment indicators, via satellite-derived land cover datasets and Land Surface Temperature (LST). The results revealed that mean annual temperature and thermal stress in Ethiopia had steadily increased over the last four decades. The DI value (> 32) indicates very high heat stress areas across the rift valley, particularly along the Danakil Depression. The area extent raised in 2023 sevenfold compared to 1984, while the extent of comfortable zones decreased by 25%. DI and WBGT values are higher in urbanized and forest-depleted areas (Southeast) and lowland regions, this was driven by climate change and induced LULC. The warming trend is currently increasing in highland areas that were formerly cooler. The WBGT results support DI outcomes, showing an increase in heat stress, expansion of high-risk areas (≥27.7 °C), and a decrease in cold stress regions. The expansion of heat stress zones is due to the compound effects of climatic warming, natural vegetation reduction and urban expansion. The findings show that heat stress is spreading across Ethiopia, increasing health risks, limiting everyday activities, and affecting socioeconomic resilience. As a result, these findings emphasise the need for climate-sensitive design, heat adaptation measures, and public health involvement in decreasing rising heat dangers.

Keywords: DI**,** Ethiopia, LULC, Thermal Stress, WBGT

Received: 5 February 2026; accepted: 6 May 2026; revised: 22 May 2026

[1] Selale University, Department of Horticulture, Collage of Agriculture and Natural Resource, Fiche, Ethiopia, ORCID ID: https://orcid.org/0000-0002-4326-0481, email: ayehufekadu5@gmail.com
[2] Selale University, Department of Horticulture, Collage of Agriculture and Natural Resource, Fiche, Ethiopia, ORCID ID: https://orcid.org/0000-0002-28197875, email: belewbekele@yahoo.com

Introduction

Climate change and global warming have significantly impacted human living environments; primarily through land use and land cover change (LULC), urban development expansion, and spikes in land surface temperature (LST) in the event of plant loss (Giannaros et al., 2014; Steeneveld et al., 2011). Rapid urbanization due to population pressure and the expansion of agricultural land has significantly contributed to heat stress all over the world (Xu et al., 2017). Outdoor activities have been curtailed as a result of increased thermal discomfort caused by air, land surface temperature increase, due to many factors and land cover change in various parts of the world (Sen & Nag, 2019). Several heat stress situations in the world are currently affecting human activity, and determining and indicating this stress level is mandatory (Sen & Nag, 2019; Steeneveld et al., 2011). This expansion of urban areas due to the growing population and the reduction of vegetation cover on the Earth's surface intensify heat stress in a maximum condition(Giannaros et al., 2014).

Several tools, including American Society of Heating, Refrigerating and Air-Conditioning Engineers(ASHRAE), Universal Thermal Climate Index(UTCI), Wet-Bulb Globe Temperature (WBGT) and Discomfort Index (DI), are commonly employed to assess human discomfort levels(Stroppiana et al., 2012). ASHRAE and UTCI are methods for calculating heat stress levels that require more variable as an input (Zare et al., 2018). However, from the aforementioned technique, the discomfort index (DI) and wet bulb globe temperature (WBGT) thermal indicators are significantly used worldwide to quantify human thermal experience by integrating temperature and humidity, as well as to predict the change in heat strain over a long period of time for a large area (Giannaros et al., 2014).

Approximated Wet-Bulb Globe Temperature (WBGT) is one of the most often used heat stress indices (Thornton et al., 2009). WBGT is primarily used to measure occupational-related heat stress, which occurs when the human body is unable to cool itself from heat generated by work, environment, or other protective materials such as clothing, resulting in exhaustion and stroke. Thus this climatic condition may require additional hydration and environmental modification to manage the stated risks (Lin et al., 2025; Zare et al., 2020). The risk is primarily related to the combination of wind speed, air temperature, LST, humidity, and sun radiation, rather than a simple assessment of human thermal discomfort (Xu et al., 2017).

Discomfort Index is a simple measure of human thermal discomfort which is related to air temperature, LST and low relative humidity driven by vegetation loss (Sen & Nag, 2019; Zare et al., 2020).Thus most people in the country experienced a significant Discomfort life experience(Mustafa et al., 2020). This has affected and, reduced work efficiency, and may be exposed to a potential health risks like heat stress and heat exhaustion, this creates a risky condition for children, and outdoor workers activities (Stroppiana et al., 2012).

The land cover change in the Sub-Saharan region, particularly in Ethiopia, exposes and reduces the total wellbeing of the nation as a result of urban development, environmental pressure and LULC, this increase the discomfort level of the people (Balas

et al., 2023; Gule et al., 2023). On the other hand, the distress level in the country which caused by aggravating factors such as LULC and temperature change, is not well documented and estimated (Gebeyehu et al., 2023; Gule et al., 2023; Mohammadian et al., 2019; Zare et al., 2018) and also a limited empirical recorded in the country in which the evidence, on how these changes have influenced human thermal comfort over time (Gule et al., 2023). As a result, addressing this gap in Ethiopian context is essential for identifying the problems to taking appropriate action. The Land Surface Temperature (LST) is an essential environmental parameter that has many uses to indicate thermal comfort (Zare et al., 2018). This can be estimated by remote sensing instruments, such as thermal infrared sensors on-board satellites, which provide the means to capture LST data on a global scale (Hagos et al., 2016a). This LST has a direct relation with air temperature and can be used to measure the temperature of the surrounding air and Relative humidity because these climatic variables have a high correlation with the local climate dynamics, particularly surface and near-surface temperatures (Balas et al., 2023).

This study looks at heat stress and vegetation cover to see if switching the LULC to a different landscape category impacts the stress response to temperature. Furthermore, this study used land-sat images to estimate air temperature and humidity, which were then used to fill in the gaps caused by a lack of gauge stations in countries such as Ethiopia. This study looks at heat stress and vegetation cover to see if altering the LULC to a different landscape category influences the stress response to temperature. So, this study builds on the previous study by indicating the effects of land-climate interaction on human comfort in the Sub-Saharan Africa region and providing strong evidence to policymakers in the country. As a result, the purpose of this study was to estimate and assess the effect of land use and land cover change on land surface temperature, as well as the impact on human thermal comfort over four decades in Ethiopia, using the instrument wet bulb globe temperature (WBGT) and discomfort index (DI) indices, with the specific goals of: (1) determining geographical and temporal variations in LULC; (2) assessing LST variability; and (3) estimating and mapping discomfort levels.

Material and methods

Study area. The study was conducted in Ethiopia which is located under sub-Sahara East-Africa situated between 3°N-15°N and 33°E-48°E (Fig. 1). The area has experienced substantial temperature variability due to LULC. The overall topography of the area is varied which consists of, hot arid (<500 m a.s.l), warm semi-arid (500-1500 m a.s.l), cool and humid (1500-2300 m a.s.l), cool sub-humid (2300-3200 m a.s.l), and cool and moist (>3200 m a.s.l). The country's topographic differences over short distances produce a wide range of climates, from semi-arid deserts to humid and temperate regions(Hagos et al., 2016a).

Data used. During the dry season, 90 images from Landsat (Landsat 5, and Landsat 8) data for the years 1984, and 2023 were downloaded. These images were acquired in the main season on December 24, 26, 1984, and December 18, 22 – 2023 at the time when the cloud coverage low (0.00 – 4.00) for 1984, and 2023, respectively.

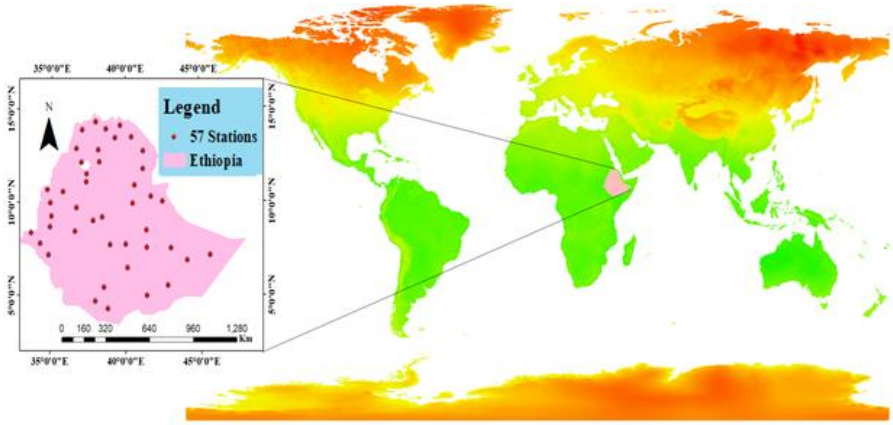

Fig. 1. Study area

Source: own study – based on databases for a study area map that reflects worldwide, African, and Ethiopian databases, focusing on Ethiopia as a whole

All images were geo-referenced and projected to the three (36, 37, and 38) Universal Transverse Mercator (UTM) Zone. This time was selected because of high LULC occurred and December is one of the hottest months in Ethiopia. Additionally Metrological Data from Ethiopian metrological Agency for the Year 1984 and 2023 from representative of 57 station (hot arid, warm semi-arid, cool and humid, cool sub-humid, and cool and moist area) were collected.

Data processing and **Land used land cover classification.** To Examine the land cover change effect on temperature increment Via on the impact of thermal stress, the land use land cover change (LULC) classification was done using ENVI (Environment for Visualizing Images) and GIS(10.5) tools. Accordingly we made rectified processes (Geometrically rectified and atmospheric FLAASH correction)(Matthew et al., 2002), to remove the atmospheric influence on the image to make true surface characteristics of the Landsat images. The majority of the images were taken in clear weather, but to remove some atmospheric and surface-related effects (for noise reduction), data were processed using a rectified processes approach (Geometrically rectified and atmospheric Fast Line-of-sight Atmospheric Analysis of Spectral Hyper-cubes correction, FLAASH) by the Environment for Visualizing Images (ENVI 5.1) and GIS (10.5) environments (Balas et al., 2023; Sim et al., 2024). The low resolution bands (Band 6 from TM and Band 10 from TIRS) were resampled to 30m resolution for high and equal image quality because the TM thermal band has a spatial resolution of 120 meters and a noise level equivalent to an LST difference of 0.5°C. A total of 120 Landsat scenes were mosaicked to cover the entire territory of Ethiopia for each reference year (Avdan & Jovanovska, 2016; Chen, 2021). The study used both the NDVI value according to user-defined value classes (particularly for forest and agriculture) and the maximum likelihood classification algorithm for varying closer and slightly similar value classes (water, bare land, and buildings) because the combination provides superior accuracy (Balas et al., 2023; Ullah et al., 2023).

Land surface temperature calculation (LST). Temperature data is recorded as digital values on Landsat 5 band 6, TM bands 10 and 11, and Landsat 8 TIRS. The

Landsat 5 TM rescaling approach ranges from 0 to 255 bytes, therefore the remote sensing system assigns the DN value to a binary integer in the pixel variable. However, the Landsat 8 OLI/TIRS sensor saves this data as DNS in the range of 0 to 65536 bytes(Mustafa et al., 2020). To convert the DN and estimate the final LST, we used the ArcGIS spatial analysis tool following the methodology given below:

Step 1. Digital numbers to TOA spectral radiance conversion from Landsat-5TM images. The Landsat 5 TM sensor saves temperature data in Digital Numbers (DN). Landsat 5 TM radiance is converted using the Top of the Atmosphere (TOA) spectral radiance scaling approach (Equation 1), which is superior to the gain and bias method (Chen, 2021; Mustafa et al., 2020; Ullah et al., 2023).

$$L_\lambda = \frac{LMAX\,\lambda - LMIN\lambda}{\text{Q calmax} - \text{Q calmin}} X(\text{Q cal} - \text{Q calmin}) + LMIN_\lambda \quad (1)$$

Where:
L_λ is the cell radiance value
QCAL is digital number (Band 6 TIFF thermal image)
LMINλ represents spectral radiance scaled to QCALMIN
LMAXλ is the spectral radiance scales to QCALMAX
QCALMIN is the calibrated quantized minimum pixel value (normally 1)
QCALMAX denotes the maximum quantized calibrated pixel value (typically 255).

Step 2. Digital numbers from Landsat-8 images are converted to TOA spectral radiance. The Landsat 8 thermal infrared sensor (TIRS) has two thermal bands, Bands 10 and 11; however, Band 11 has a greater calibration uncertainty; thus, I employed just Band 10 for this technique, as recommended by the USGS (Mustafa et al., 2020; Ullah et al., 2023). Based on this, a split-window technique was employed to convert the DN value to TOA spectral radiance using Equation 2:

$$\text{TOA}\ (L_\lambda) = M_L * Q_{cal} + A_L - O_i \quad (2)$$

Where:
L_λ is represents the TOA spectral radiance in watts/(meter squared ∗ ster ∗ μm)
ML indicates a metadata-based multiplicative rescaling factor (Radiance_Mult_Band=0.0003342)
Q_{cal} is band 10 (band 10 Tiff image from the land sat 8 thermal infrared sensor TIRS) and The metadata specifies the band-specific additive rescaling factor is AL (RADIANCE_ADD_BAND_10=0.1000). Furthermore, the value of Band 10 has been adjusted by 0.29°C

Step 3. Calculate the brightness temperature. Following spectral radiance conversion, the two thermal bands, Band 6 (TM sensor) and Band 10 (TIRS sensor), were converted to brightness temperature. This allowed for the measurement of the thermal calibration constant and spectral radiance, which were then translated to Celsius using a comparable approach (Matković et al., 2024), Equation 3:

$$T(BT) = \frac{K_2}{In(\frac{K_1}{L_\lambda} + 1)} - 273.15 \quad (3)$$

Where:
BT is the satellite brightness temperature in Celsius, of Band 6 and 10

K_1 is calibration constant one 607.76 for TM and 774.8853 for TIRS that represent thermal conversion from the metadata

K_2 is calibration constant two which is 1260.56 for TM and 1321.0789 for TIRS which represent thermal conversion from the metadata

L_λ is represents the TOA spectral radiance in watts/(meter squared ∗ ster ∗ μm).

Step 4. NDVI calculation for the input of P_V calculation. Vegetation cover percentage is very important for estimating an object's ability to emit energy relative to a black object with the same temperature based on the minimum and maximum values because land surface emissivity is the main factor of temperature variability in surfaces, so this was calculated using NDVI, the most commonly used vegetation index for observing greenery globally and the best approach for vegetation projection (Nam et al., 2024). To calculate NDVI, Equation 4 was used with the conditional Float approaches based on the formula below(Mansourmoghaddam et al., 2022). The Arc GIS spatial analysis tool (Map algebra) was applied to calculate the vegetation proportion (Pv), which is strongly related to the NDVI, and the emissivity (ε), which is also related to Pv.

$$\text{NDVI} = \frac{Float(NIR-Red)}{Float(NIR+Red)} \quad (4)$$

Where:

NIR and RED refer to the reflectance's of the near-infrared (NIR) and red bands, respectively, fortunately the input varies based on sensor types:

For TM sensor $$NDVI = \frac{Float(Band4-Band3)}{Float(Band4+Band3)}$$

For OLI/TIRS sensor $$NDVI = \frac{\text{Float}(\text{Band5}-\text{Band4})}{\text{Float}(\text{Band5}+\text{Band4})}$$

Step 5. The proportion of vegetation (P_V) calculation. For calculating P_v, the NDVI image minimum and maximum values were used as an input (Neinavaz et al., 2020) in Equation 5.

$$P_v = \left(\frac{(NDVI-NDVI_{min})}{(NDVI_{max}-NDVI_{min})} \right)^2 \quad (5)$$

Where:

NDVI: The NDVI Tiff image is used as input for the spatial analysis tool (Map algebra), and NDVI min and max represent the image's minimum and maximum values, respectively

Step 6. Emissivity (ε) calculation. Emissivity (ε) was calculated based on, P_v and by the corresponds correction value of the equation (0.986) (Chakraborty et al., 2015; Gohain et al., 2021; Zhang et al., 2013) by the Equation 6.

$$\varepsilon = 0.004 * P_v + 0.986 \quad (6)$$

Where:

Proportion of vegetation is represented by Pv, and the standard emissivity correction value for vegetation is 0.986, and it serves as a correction factor. Furthermore, because the TM and OLI pixels contain multiple land covers, and then I calculate the vegetation proportion associated with each land cover and then scale the PV of that land class in a pixel by 0.004 of another standard value.

Step 7. Calculating the land surface temperature (LST). The land surface temperature (LST) is the radiative skin temperature of the land surface, as measured by a remote sensor pointed in the same direction. It is calculated using top-of-atmosphere brightness temperatures derived from the infrared spectral channels of a geostationary satellite constellation. Equation 7 was used to compute land surface temperature (LST)(Mustafa et al., 2020; Neinavaz et al., 2020).

$$\text{LST} = \frac{BT}{1+\left(\frac{\lambda . BT}{P}\right)} Ln(\varepsilon) \quad (7)$$

Where:
The term BT refers to the highest atmospheric brightness temperature (˚C)
ε is the land surface Emissivity
λ=wavelength of emitted radiance wavelength of emitted radiance taken as 10.895 (0.60+11.19/2) for Band 10 (OLI-TIRS) and 11.45 (10.40+12.50) for Band 6.
P = h ×c / σ = always use as a value = 1.4388 (1.438×10^{-2} mK)
Where:
h=Planck's constant (6.626 X 10-34 J/s)
σ=Boltzmann constant (1.380649 X 10-23 J/K) and
c=velocity of light (2. LST 9.98 X 10^8 m/s).

Step 8. Standardization of the computed value (LST). After extracting a representative value from the image with the ArcGIS extraction tool, LST normalization was applied to guarantee that all variables were in good proportion. This was done to adjust for changes in sensor images, seasonal variations, and topography variables caused by the thermal image's mountainous backdrop (Balas et al., 2023). Equation 8 was used to correct epoch-specific errors during the LST standardization process.

$$\text{LSTs} = \text{LST} - \frac{LST_u}{LST_{\boldsymbol{\Omega}}} \quad (8)$$

Where:
LSTs=Standardized LST, LSTu refers the average of expected LST from 1999 to 2019 and LST
Ω=Standard deviation of LST from 1999 to 2019.

Change detection and classification:

LULC change analysis. The over-time study of detection is crucial for understanding temporal changes in land use and land cover patterns, as well as their effects on climate dynamics. For this, pre and post-classification change detection approach, NDVI value-based classification was used to monitor the extent of land cover shift to another land cover, as well as to explore the transformation effect occurring among different land use and land cover types (Chughtai et al., 2021; Wei et al., 2021).

Classification of Land surface temperature. Jenks' natural breaks strategy was used to classify temperature by decreasing variance within the classes and maximizing variance between classes to determine the optimal arrangement of values into discrete classes(Şahin et al., 2025; Tan et al., 2020).

Estimation of human thermal comfort. Thermal comfort was calculated using category two bio-meteorological indices, which do not take into account human thermal

physiology and are referred to as "simple" keys: the Discomfort Index (DI) and the Approximated Wet-bulb Globe Temperature. Furthermore, these two indices only consider the effects of air temperature and humidity, omitting other variables such as mean radiant temperature and wind speed, and do not include thermal physiology; nevertheless, they were chosen for this study because they are easily validated using the available observational data(Xu et al., 2017). A widely used DI index suggested by Thom (Thom, 1959) was used to express the thermal comfort as indicated in Equation 9.

$$DI = Ta - 0.55 * (1 - 0.01 * RH) * (Ta - 14.5) \quad (9)$$

Where:

Ta is the air temperature (C) and RH the relative Humidity (%) and to replace Ta with directly remotely-sensed thermal derived LST cannot given a good interpretation to calculate DI because LST is the radiometric temperature of the surface but T air tells you how hot the air is for people; however using both gives comprehensive data for thermal comfort analysis (Shen et al., 2020). Furthermore, obtaining reliable air temperature and relative humidity from remote sensing data is problematic since there is no practical and reliable method for directly converting remote sensing data to air temperature or relative humidity.

Furthermore, obtaining air temperature and relative humidity data for the entire country of Ethiopia is difficult because air temperature and relative humidity are usually calculated from measurements taken at meteorological stations, but the country's metrological station count is relatively restricted. We employed a common method to calculate the main two human thermal comfort indices, by applying the model provided by (Xu et al., 2017). First estimation of LST from remotely-sensed thermal infrared information followed by Retrieval of air temperature using Arc GIS Spatial analysis raster Calculator based Equation 10, and relative humidity Equation 11:

$$Ta = -0.0012\,LST^2 + 0.1811\,LST + 31.016 \quad (10)$$

$$RH = -0.0008LST^3 + 0.1093LST^2 - 5.0429LST + 125.63 \quad (11)$$

WBGT (Approximated Wet-bulb Globe Temperature) is an index that can be used for evaluating outdoor thermal stress conditions. This can be computed using Steeneveld et al. (2011) formulated linear model Equation 12:

$$WBGT = 0.567 * Ta + 0.393 * e + 3.94 \quad (12)$$

Where:

Ta is air temperature (°C, Retrieved above)

e is water vapour pressure (hPa). For Estimation of water vapour pressure, many studies used a Goff-gratch, or Buck equation, but this is mostly complex equation used in the fields on over ice and water which is dominantly uses air temperature as input (Shen et al., 2020). But August-Roche-Magnus approximation are able to estimate saturation vapor pressure with directly modelling from remotely-sensed thermal derived LST. Therefore we used this equation to estimate the saturation vapor-pressure by using August-Roche-Magnus approximation by Arc GIS Spatial analysis raster Calculator tools based Equation 13:

$$e = 0.6107exp\left(\frac{17.38xT}{239.0+T}\right) \quad (13)$$

Where:
e is denotes the saturation water vapour pressure (hPa)
T is denotes the LST in °C.

Accuracy assessment:

Accuracy assessment of LULC classification. The measurements we utilized to ensure that the classified image accurately reflected the truth available on the ground. The kappa coefficient and overall accuracy were calculated by dividing the number of correctly categorized pixels by the total number of samples obtained from 500 GPS pixel points(for 2023), Google Earth image(for 1984).

Assessment of LST Accuracy. The value was validated using the T-based technique (Tan et al., 2020), which involved comparing LST-derived air temperature to in situ ground measurements generated from long-term temperature data gathered from Ethiopia's National Meteorological Agency (NMA) 57 gauge stations located across the country. Following point-by-point demonstration, correlation accuracy, bias analysis and root-mean-square error were used Equation 14, to compare the findings of computed LST and gauge station data.

$$RMSE = \frac{\sqrt{Ta\ sensors\ derived\ -Ta_{insitu}}}{N} \quad (14)$$

Where: RMSE is root-mean-square error and N is number of sites.

Validation of the satellite-estimated DI, **WBGT, air temperature and relative humidity.** The validation of the satellite-based predicted DI and WBGT, as well as air temperature and relative humidity, was carried out using measurements from 57 meteorological stations, as with others(Clark & Konrad, 2024; Liu et al., 2026).

Grading thermal comfort levels based on Climatic dynamics in the instance of LULC. Thermal comfort grading is a method of categorizing indoor and outdoor habitats based on projected occupant enjoyment, using criteria established by international standards and indices. As a result, threshold values for DI and WBGT standards were established, with varied grading categories, and so thermal comfort levels of DI and WBGT were classified based on the following clear-cut value (Table 1). Accordingly, the study technique was done based on the following flowchart (Fig. 2).

Table 1. Thermal Index grading categories

Thermal Index	Category in °C							
	Extreme Heat Stress	Very Strong Heat Stress	Strong Heat Stress	Moderate Heat Stress	No Thermal Stress	Slight Cold Stress	Moderate Cold Stress	Reference
DI	29-32	27-39	24-27	21-24	<21	10	5≤10	Thom, 1959
WBGT	≥ 32.2	31.1-32.1	29.5-31	27.8–29.4	12≤ 27.7	2-12	2	Lin et al., 2025

When DI>32 and WBGT>32.2 termed as Dangerous heat stress lead to severe health outcomes or State of medical emergency.

Source: Lin et al., 2025; Thom, 1959

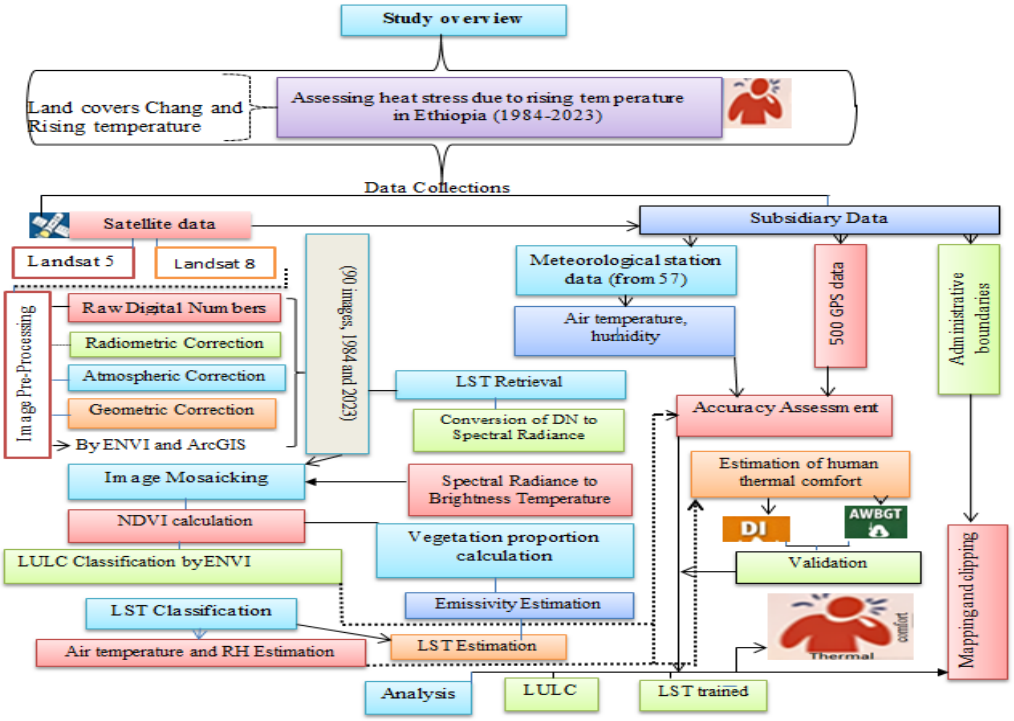

Fig. 2. Methodological procedure

Source: own study used integrated methodological approach such as climatic data, remote sensing techniques, land cover classification, and thermal comfort assessment models to investigate the spatial and temporal links between environmental change and human thermal stress

Results and discussion

We used in-situ meteorological measurements and GPS data points from 1984 to 2023 to validate the estimated LULC, LST, DI, and WBGT based on satellite estimates. The study discovered a strong positive correlation ($r > 0.90$) between satellite-derived values and station-based measurements of air temperature and relative humidity. This high correlation indicates good consistency and a strong linear link between satellite-derived estimates and in situ ground record data. Furthermore, RMSE and MAE values were low, reflecting the little differences between satellite-based estimations and ground-measured LULC, LST, DI, and WBGT indices. Therefore, the low error value confirms the projected heat discomfort. Indices can be used to investigate heat stress occurrences from 1984 to 2023 in the context of LULC consequences.

The LULC analysis from 1984 to 2023 revealed a significant decrease in plant cover, which was primarily converted into other land use types (Table 2 and Fig. 3). The land surface temperature (LST) rose from 1984 to 2023 as a result of the LULC shift (Fig. 4). The maximum temperature has risen from 44.87 °C in 1984 to 46.98 °C in 2023. Land surface temperature (LST) is a commonly used indication of energy flow in interactions between the land surface, atmosphere, and biosphere. This was due to vegetation reduction, in which, in 1984, the forest cover of the entire country was 31.02%, but this has subsequently fallen and decreased to 12.66% in 2023.

Table 2. LULC area in 1984 and 2023

LULC	1984 Area km^2	2023 Area km^2	Change (%) 2023-1984
Lakes	7612	8048.0	0.036
Built-up, Rocks and Bare soil	410614.8	478923.5	5.69
Crop, grass, shrubs and agroforestry	409709.9	561123	12.61
Open Forest	242318.5	139123	-8.59
Dense Forest	129744.5	12782.4	-9.746

Source: own study on Land Use/Land Cover (LULC) area extent and percentage change in Ethiopia from 1984 to 2023

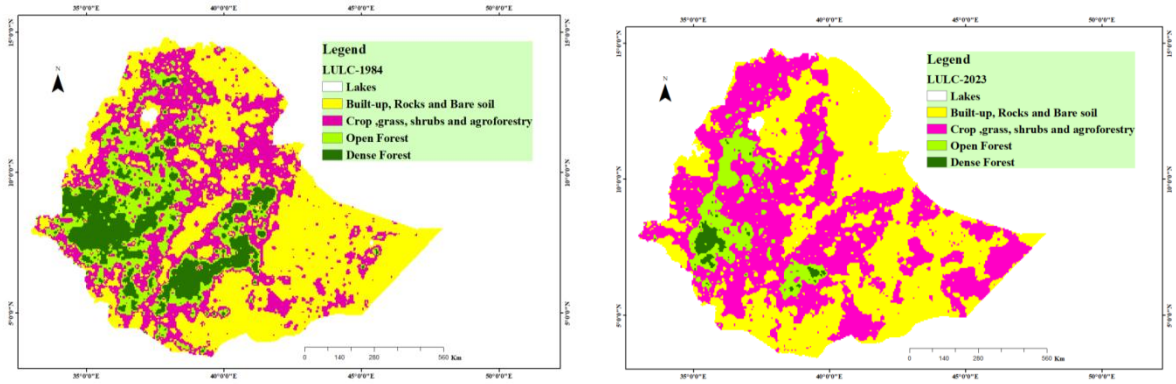

Fig. 3. LULC 1984 and 2023
Source: own study using GIS and ENVI classification tollse for Comparison of Land Use/Land Cover (LULC) patterns in Ethiopia between 1984 and 2023, exhibiting temporal fluctuations across main land cover classifications

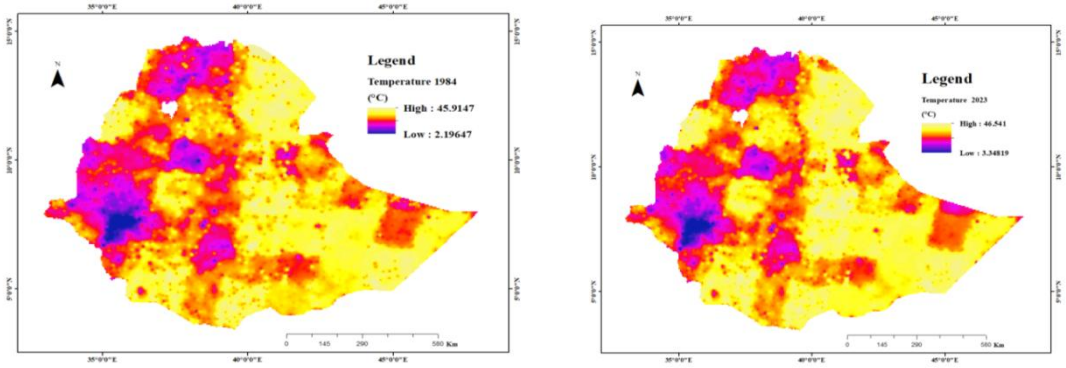

Fig. 4. Temperature variation in 2023 from 1984
Source: own study indicating Temperature variation in 2023 compared 1984 demonstrates temperature trends across different land cover categories, highlighting how warming patterns alter over time

Trends of Discomfort Index (DI) from 1984 to 2023. The increase in temperature caused by LULC had an impact on Ethiopians' general comfort and social wellbeing. The DI value showed that the discomfort from moderate to severe heat stress increased by 8.3% between 1984 and 2023, which is closely related to the rise in surface and air temperatures caused by plant loss and land use change. These findings showed that previously vegetated areas now suffer higher levels of thermal stress, especially in areas that have been transformed to urban and empty lands. The category of Very Strong heat stress increased by 7.2% during the last four decades, suggesting that the LULC transformation has resulted in a significant shift in thermal conditions, potentially harming human comfort and productivity in Ethiopia. Extreme heat stress has significantly increased (2.2%), covering a larger area (34572.93 km^2) than in 1984 (6125.9 km^2), negatively impacting the population's daily activities, food security, and sustainable development strategy (Table 3). This DI increase is strongly associated with LST, via air temperature, and low relative humidity caused by plant removal. This indicates that changes in LULC have an expected impact on present temperature conditions and human comfort levels. The incremental value indicated that the majority of people in the country had a significant thermal discomfort life experience, which impacted and reduced work efficiency, and may have been exposed to potential health risks such as heat stress and heat exhaustion, which can create a dangerous situation, particularly for children and outdoor workers.

Table 3. Heat stress changes area extent based on discomfort category from 2023 to 1984

Di-1984 extent (km^2)	Di 2023 extent (km^2)	Category in °C	Stress type
8655.632512	6051.50288	1-9	Moderate Cold Stress
1760.887777	1835.292112	9-10	Slight Cold Stress
362990.9437	275293.7654	10-21	No Thermal Stress
327574.7745	275740.1821	21-24	Moderate Heat Stress
339380.1642	372663.4272	24-27	Strong Heat Stress
57811.69107	138142.9025	27-29	Very Strong Heat Stress
3298.564798	25024.45134	29-32	Extreme Heat Stress
2827.341426	9548.476468	32-37.8	State of medical emergency
1104300	1104300		

Source: own study indicating-Changes in heat stress area extent per discomfort category(DI) from 1984 to 2023 it depicts the area extent of various heat discomfort levels over time, demonstrating changes in the distribution and intensity of heat stress categories

Contribution of the major land cover changes to DI. The land cover categories and DI values differ depending on plant cover and inverse correlation. Higher grade values were reordered in regions recently converted to built-up (DI < 27 ◦ C), followed by agriculture and bare lands. This illustrated how LULC changes influence and create discomfort in persons, potentially leading to greater LST and air temperatures. The LULC data revealed large changes between 1984 and 2023, primarily owing to vegetation loss and conversion to other land use types such as built-up areas. The rate of change was quite high over the last four decades.

A comparison of LULC extent from 1984 to 2023 shows that areas once dominated by vegetation have considerably decreased. Likewise, the Discomfort Index (DI) increased by more than 12.34% over the same time frame. This increase in DI is highly correlated with the observed increase in air temperature following plant removal. The findings clearly demonstrate that changes in land cover have had a discernible impact on local temperatures and human comfort levels. Land, and bare land, with heat change being the most prevalent and potentially exacerbating health-related issues in these areas. This change reflects fast land cover change during the last four decades.

Trends of Approximated Wet-Bulb Globe Temperature (WBGT) from 1984 to 2023. Approximated Wet-Bulb Globe Temperature is predominantly slow Work-related heat stress occurs when the human body is unable to cool itself due to heat created by the workplace, environment, or other protective elements such as clothes, resulting in exhaustion and stroke(Liu et al., 2026). To handle the aforementioned dangers, this climatic situation may require additional hydration and environmental change (Carter et al., 2020). This risk is mostly caused by the combination of wind speed, air temperature, LST, humidity, and sun radiation, rather than a simple measurement of human thermal discomfort (DI) (Chakraborty et al., 2015). From the analysis's the WBGT (Table 4) revealed that Moderate Heat Stress was increased by 102.4% (1066.4 km^2) in 2023 as compared to 1984, in addition Dangerous heat stress rises by 64% (1710.9 km^2) and Extreme Heat Stress by 24.5 (669.2 km^2), Strong Heat Stress by 21.04% (198.4 km^2) and Extreme Heat Stress by 24% (24.8 km^2), this indicated that the thermal disturbances affects the working condition and suggested that that workers are frequently exposed to thermal conditions that can reduce comfort and productivity represents substantial percentage of time when workers are at increased threat of heat-related tension. From the total area of the country, 1710.9 km^2 characterizes serious situations where direct medical intervention may be required to prevent severe heat illness. Based on observations, it is clear that this area is categorized under the state of medical emergency category.

Table 4. Spatiotemporal extent of human heat stress types by WBGT category from 1984 to 2023

AWBG1984area (km^2)	AWBG 2023area (km^2)	Category in °C	Steers type
18600.98866	15351.9686	5.46-12	Slight Cold Stress
1080515.32	1077935.691	12-27.7	No Thermal Stress
1041.675167	2108.105473	27.7-29.4	Moderate Heat Stress
942.4678946	1140.856855	29.4-31	Strong Heat Stress
768.8557651	769.235999	31-32.1	Very Strong Heat Stress
99.20727258	124.0057123	32.1-32.2	Extreme Heat Stress
1041.675167	1710.887806	32.2-33.2	Dangerous heat stress
1104300	1104300		

Source: own study indicating-Changes in heat stress area extent per discomfort category(AWBG) from 1984 to 2023 it depicts the area extent of various heat discomfort levels over time, demonstrating changes in the distribution and intensity of heat stress categories

Human thermal comfort based on DI Class mapping. The findings revealed that between 1984 and 2023, a wide range of human thermal discomfort conditions were observed in Ethiopia. According to the levelled DI map (Figs. 5 and 6), an extremely high DI value (32-36.8°C) was observed in 1984 in Dallol within the Danakil Depression, which covered 3298.6 km^2. However, this level rose sevenfold, with the extent of 25024 km^2 in 2023, including several adjusted areas following the lowland valley. Climate change and volcanic activity have contributed to this high heat, with temperatures frequently exceeding from predictions, causing dehydration and heat-related ailments. This is similar to some findings in the world (Yeo et al., 2021) and in Ethiopia (Hagos et al., 2016b). This area is expected to be challenging, particularly for outdoor workers, the elderly, and persons with underlying health concerns; productivity and physical performance are likely to deteriorate severely at this degree of discomfort.

In 1984, areas with no thermal stress covered 362990 km^2, but this decreased by 25% to 275293 km^2 in 2023. The moderate value, which suggests some discomfort, spanned 327574 km^2 in 1984 but reached 275740 km^2 four decades later. In this category, the human body can regulate the condition in an acceptable manner with minimal danger for brief exposure. The cold temperature exposure (moderate to mild cold stress) was reduced by 25%, but the terminal stress area extent (no to moderate stress) rose by 20%. On the other hand, the higher temperature zone (strong to intense heat stress) has grown by 35% and currently accounts for more than 49.3% of the country's total area (2023), compared to 1984. Other studies found that many factors increase thermal stresses in many parts of the world as a result of LULC effects (Shen et al., 2020), exacerbating the Urban Heat Island (Chakraborty et al., 2015; Zare et al., 2020). Warm weather and sunlight have a substantial impact on the utilization of outdoor activities (Berglund, 1980; Steeneveld et al., 2011). Many studies also indicated vegetation coverer had a significant effect on the LST because LULC aggravates the LST, which reduces human comfort (Steeneveld et al., 2011; Xu et al., 2017).

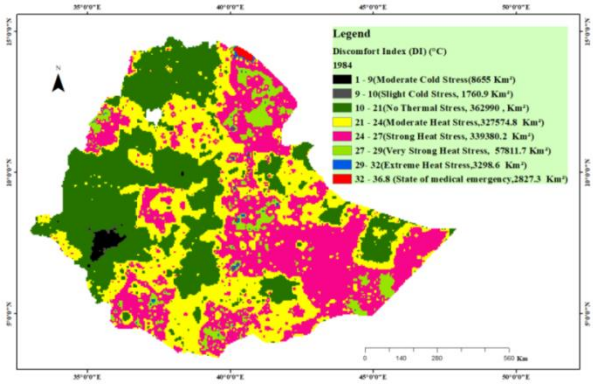

Fig. 5. Discomfort Index (DI) categories 1984

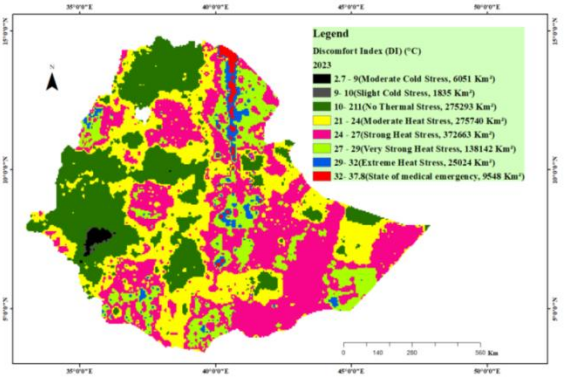

Fig. 6. Discomfort Index (DI) categories 2023

Source: own study classified by GIS that showing Discomfort Index (DI) categories in 1984 (Fig. 5) and 2023 (Fig. 6), showing the distribution and comparison of thermal discomfort levels between the two years and highlighting changes in heat stress conditions over time

Spatiotemporal pattern of thermal stress by DI category. The spatiotemporal change raises the risk level from low to high, with higher DI classes indicating public health concerns (Figs. 7 and 8), as well as decreased labour productivity and general population well-being (Table 5). The results showed that the number of extremely dangerous and uncomfortable regions increased significantly in 2023, reaching 2827.3 km^2. This extends far beyond the earliest depression area of the Great Rift Valley of Afar Region; in such conditions, all outdoor activities, including physical work, are disproportionately affected. Furthermore, some areas in this region require medical attention and immediate heat adaption techniques. From 1984 to 2023, the frequency and duration of moderate cold heat stress decreased (-0.24%), but strong heat stress (3%), very strong heat stress (7.2%), and extreme heat stress (1.96%) increased. This trend indicates that uncomfortable and unsafe temperature settings are becoming more common. Furthermore, the number of medical crises increased by 0.67% in 2023, increasing the risk of illness for vulnerable populations, as heat stress increased as a result of dehydration, and heart stress may worsen as a result of this change, which also shortens the body's recovery time and increases total heat exposure .This argument was consistent with the fact that warm weather and sunlight have a significant impact on the utilization of outdoor spaces, and clear skies are also favourable for outdoor activities (Imran et al., 2022).

Heat stress varies spatially; higher DI levels have frequently been seen in the country's highlands and rural areas in the southeast and west, where deforestation and development have lately occurred. This showed that metropolitan areas, as well as former extremely hot spots, sustained strong to severe heat stress, most likely due to the urban heat island effect, heavy infrastructure, and insufficient natural cover. However, the bulk of highland areas continue to experience pleasant to moderate heat stress, with current trends indicating a steady increase in discomfort rating even in these usually cooler zones. Furthermore, the expansion of greater DI extent extends into previously comfortable places shows that human heat pressure becoming a global occurrence. So this spatial heat stress expansion exposes the sensitivity of civilizations that lack adaptive control measures; this indicates that access to green space in urban areas and vegetation cover in degraded areas is critical as heat-resilient approaches. This finding is consistent with many studies in which that discomfort condition was increased due to climate change and other relevant factors (Khovalyg et al., 2020; Nam et al., 2024; Sen & Nag, 2019; Steeneveld et al., 2011) The spatiotemporal change increases the temperateness, thereby increasing heat stress in many areas of the world (Giannaros et al., 2014; Lin et al., 2025; Mohammadian et al., 2019). Warm and stressful situations are more common, and extensive crossways of the Sub sharer region (Djongyang et al., 2010; Imran et al., 2022).

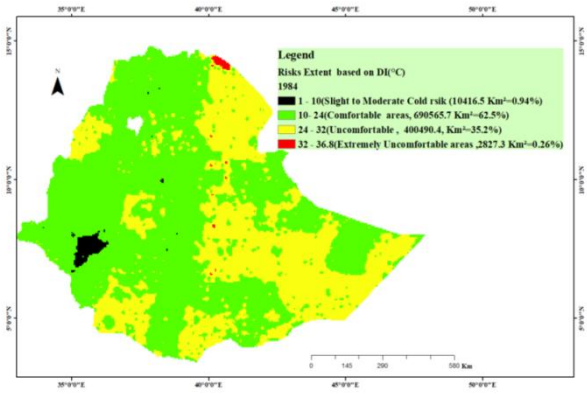

Fig. 7. Risk extent of 1984

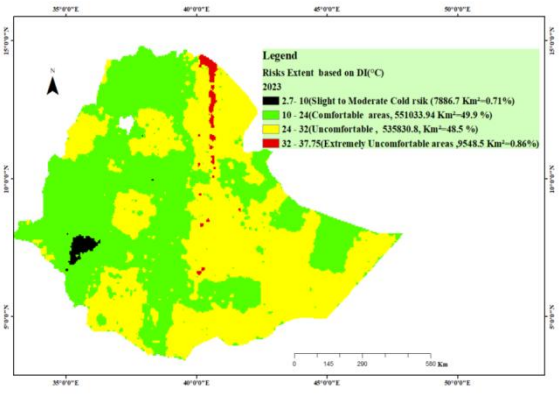

Fig. 8. Risk extent of 2023

Source: own study using DI indicators showing the spatial distribution and coverage of risk levels in 1984 (Fig. 7) and in 2023 (Fig. 8), and shows highlights variations over time

Table 5. Spatiotemporal trends of warmness

DI trend from 2023 to 1984(%)	Category in °C	Steers type
-0.235817226	1-9	Moderate Cold Stress
0.006737692	9-10	Slight Cold Stress
-7.941426994	10-21	No Thermal Stress
-4.693886842	21-24	Moderate Heat Stress
3.013969302	24-27	Strong Heat Stress
7.274401107	27-29	Very Strong Heat Stress
1.967389889	29-32	Extreme Heat Stress
0.608633075	32-37.8	State of medical emergency

Source: own study showering the Spatiotemporal trends in warmness and stress types using the Discomfort Index (DI), exhibiting variations in thermal conditions and heat stress patterns across time

Spatiotemporal distribution of thermal stress by WBGT category. The results of WBGT value revealed that human heat stress rose, which has a strong relationship to the thermal stress of the human body (Fig. 9). The map and computing value of WBGT demonstrated a clear change in human thermal stress as external heat increased. Heat-related discomfort affects 0.18% of the country (5853 km^2), with high WBGT values (≥27.7°C) (Table 6), this area poses major health hazards. LST, humidity, air temperature, and radiation heat all have a significant impact on sweating and evaporation, affecting the bodies of cooling systems. Places with WBGT values (12–27.7°C) that enable safe human activity cover an area of 1077935.7 km^2, whereas parts where thermal comfort begins to reduce and moderate heat stress may arise as a heat stress (27.7-29.4°C) cover an area of 2108.1 km^2, which grew by 0.096% in 2023 when compared with 1984. The cold temperature effect based on the WBGT values was reduced by -0.29%, demonstrating how climate changes affect air temperature due to the effect of many factors. Furthermore, the Strong Heat Stress (29.4–31°C) increased by 0.018%, while Extreme Heat Stress (31–32.1°C) raises by 0.0025%, in four decades.

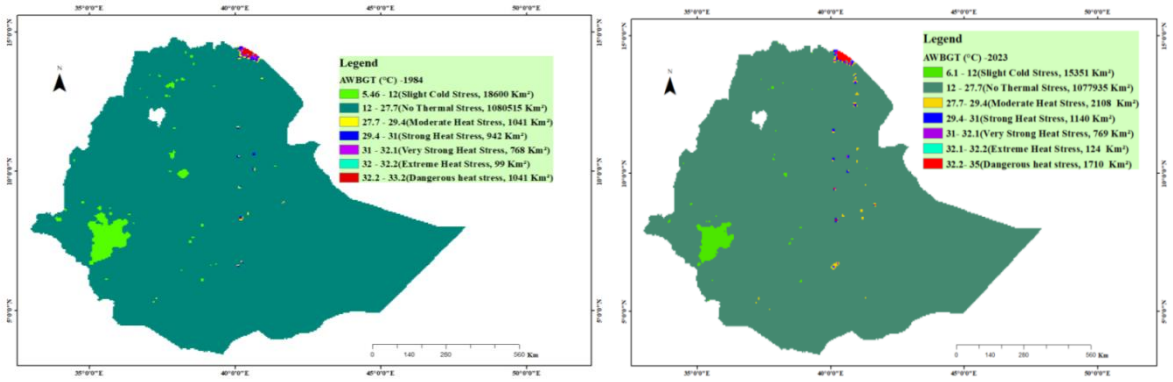

Fig. 9. Heat stress levels based on WBGT (1984 and 2023) value
Source: own study based on WBGT DI indicators showing the spatial distribution and coverage of risk levels in 1984 and 2023, and shows variations over time.

Table 6. AWBG Expansion Extent in %

WBG % extent (1984)	WBG % extent (2023)	Category in °C	Trends (2023 from 1984) %	Steers type
1.68441444	1.390199094	5.46-12	-0.294215345	Slight Cold Stress
97.84617586	97.61257729	12-27.7	-0.233598569	No Thermal Stress
0.094329002	0.190899708	27.7-29.4	0.096570706	Moderate Heat Stress
0.085345277	0.10331041	29.4-31	0.017965133	Strong Heat Stress
0.069623813	0.069658245	31-32.1	3.44321	Very Strong Heat Stress
0.008983725	0.01122935	32.1-32.2	0.002245625	Extreme Heat Stress
0.094329002	0.154929621	32.2-33.2	0.060600619	Dangerous heat stress

Source: own study indicating the AWBG expansion extent and trends from 1984 to 2023, expressed as %, demonstrating changes in spatial coverage and stress type distribution over time

However, the extreme WBGT value (> 32.2°C) covers an area of 1710.9 km^2. This class causes the body to enter a severe thermal state in which outdoor activities should be minimized or avoided since normal thermoregulatory processes may fail to regulate the body's heat stress. As a result, adaptive methods are required to prevent heat-related health hazards as temperature extremes increase (Zhang et al., 2013).

The computed stress value of WBGT across the country is directly related to the change of forest areas into other land covers, particularly into Urban and agricultural lands. This indicated that vegetation covers on the former forest region plays a great role in temperature regulation, through shading and evapotranspiration control. This explains the substantial rise in moderate and extreme heat stress conditions in 2023 compared to 1984. The increase in heat stress suggests that many areas that previously experienced comfortable or slightly cool conditions are now exposed to higher thermal pressure. Particularly, very strong heat stress can indicate difficulties in outdoor activities, labour productivity, and public health, especially in regions already vulnerable to high temperatures. These findings are consistent with prior studies demonstrating that urban expansion, deforestation, and land degradation intensify surface heating and elevate human thermal discomfort (Berglund, 1980; Giannaros et al., 2014; Imran et al.,

2022; Steeneveld et al., 2011). In addition, other studies showed that heat stress categorized as strong (29.4–31°C), very strong (31–32.1°C), or extreme heat stress (32.1–32.2°C), this carte a thermal environments stress that can make them less productive and more likely to get sick from heat or dehydration (Imran et al., 2022; Steeneveld et al., 2011; Tan et al., 2020; Thom, 1959). Also, the heat stress indicated where WBGT values are considered unsafe (> 32.2°C) shows that the stress level in the former Extremely Low Elevation (Danakil Depression) has increased and spread throughout the country, reaching 1710.9 km^2 (Fig. 9). Comparable to this study other findings showed that the uncomfortable area has grown in Africa (Morakinyo et al., 2024) and exposing many individuals to harmful conditions in Ethiopia (Hagos et al., 2016a).

Conclusions

This study employed DI and WBGT stress indicators to assess Ethiopia's thermal comfort between 1984 and 2023. The findings revealed that heat stress levels had risen throughout Ethiopia during the previous four decades. Extreme, very strong, and strong heat stress categories were expanded, resulting in a considerable fall in human thermal comfort and significantly covering the former non-heat stressed areas. The DI study discovered a considerable increase in high-risk thermal zones, notably in lowland areas like the Danakil Depression, the Rift Valley corridor, and parts of eastern and western Ethiopia. While places with low thermal stress decreased by around 25%, but, the extremely high DI class (32–36.8 °C) increased about sevenfold. Notably, more than half of the country is currently experiencing extreme heat stress. The high value of WBGT (≥32 °C) was recorded in the Depression of Afar districts, and the trend indicated an expansion of this discomfort level to the adjacent lowland areas of the rift valley, indicating an unsafe condition for daily activities. This has a great negative impact on the productivity context in the areas, which create a great burden on human survival and overall outdoor activities. The reduction of temperature in the cold highland areas and the increase of heat stress zones were due to the land uses and land cover change, resulting in deforestation and the expansion of urban areas due to population pressure, adding to the overall influence of global climate change. Land cover dynamics in the past four decades have increased surface warming and human heat stress, particularly decreasing the natural cooling by shading and evapotranspiration. Generally, the result indicates thermal discomfort and heat stress in Ethiopia in the past 40 years have increased, and the extent has become widespread, beyond the former high-risk thermal zones into previously comfortable spaces. This has a negative consequence for agricultural productivity, outdoor activity, and health-related factors. Furthermore, Increases People's vulnerability, primarily disturbs the health of elderly people, and the total health condition, and increases the frequency of disease occurrences, which dominantly affects the socio-economic resilience. As a result, this study highlights that the application of the heat mitigation strategy like afforestation urban greening, restoration of the degraded area managing and controlling of the existing vegetation

covers, climate mitigation based urban planning and expansion like green space enhancement, strengthen sustainable land management system increasing the adaptive capacity of the community are very important and critical to reduces the discomfort in related to heat-related risks, to increase productivity, and the general overall quality of life of the people in Ethiopia.

Acknowledgments and Funding Declaration

I acknowledge Salale University because this work was partially financed by Salale University's College of Agriculture and Natural Resources.

Declaration of Competing Interest

The authors state that they have no known competing financial interests or personal relationships that could have influenced the article mentioned in this paper.

Data Availability

The datasets used and/or analysed during the current study are available from the corresponding author on reasonable request.

Use of Generative AI and AI-Assisted Technologies

The Authors are not used generative AI and AI-assisted technologies in the preparation of this manuscript.

References

Avdan U., Jovanovska G. (2016). Algorithm for Automated Mapping of Land Surface Temperature Using LANDSAT 8 Satellite Data. Journal of Sensors, 2016, 1–8. https://doi.org/10.1155/2016/1480307.

Balas D.B., Tiwari M.K., Trivedi M., Patel G.R. (2023). Impact of Land Surface Temperature (LST) and Ground Air Temperature (Tair) on Land Use and Land Cover (LULC): An Investigative Study. International Journal of Environment and Climate Change, 13(10), 3117–3130. https://doi.org/10.9734/ijecc/2023/v13i102980.

Berglund L.G. (1980). Revised standards on thermal conditions for human occupancy. Habitat International, 5(3–4), 525–532. https://doi.org/10.1016/0197-3975(80)90039-9.

Carter A.W., Zaitchik B.F., Gohlke J.M., Wang S., Richardson M.B. (2020). Methods for Estimating Wet Bulb Globe Temperature From Remote and Low-Cost Data: A Comparative Study in Central Alabama. GeoHealth, 4(5). https://doi.org/10.1029/2019GH000231.

Chakraborty S.D., Kant Y., Mitra D. (2015). Assessment of land surface temperature and heat fluxes over Delhi using remote sensing data. Journal of Environmental Management, 148, 143–152. https://doi.org/10.1016/j.jenvman.2013.11.034.

Chen T.L. (2021). Mapping temporal and spatial changes in land use and land surface temperature based on MODIS data. Environmental Research, 196, 110424. https://doi.org/10.1016/j.envres.2020.110424.

Chughtai A.H., Abbasi H., Karas I.R. (2021). A review on change detection method and accuracy assessment for land use land cover. Remote Sensing Applications: Society and Environment, 22. https://doi.org/10.1016/j.rsase.2021.100482.

Clark J., Konrad C.E. (2024). Observations and Estimates of Wet-Bulb Globe Temperature in Varied Microclimates. Journal of Applied Meteorology and Climatology, 63(2), 305–319. https://doi.org/10.1175/JAMC-D-23-0078.1.

Djongyang N., Tchinda R., Njomo D. (2010). Thermal comfort: A review paper. Renewable and Sustainable Energy Reviews, 14(9), 2626–2640. https://doi.org/10.1016/j.rser.2010.07.040.

Gebeyehu A.K., Snelder D., Sonneveld B. (2023). Land use-land cover dynamics, and local perceptions of change drivers among Nyangatom agro-pastoralists, Southwest Ethiopia. Land Use Policy, 131. https://doi.org/10.1016/j.landusepol.2023.106745.

Giannaros T.M., Melas D., Daglis I.A., Keramitsoglou I. (2014). Development of an operational modeling system for urban heat islands: An application to Athens, Greece. Natural Hazards and Earth System Sciences, 14(2), 347–358. https://doi.org/10.5194/nhess-14-347-2014.

Gohain K.J., Mohammad P., Goswami A. (2021). Assessing the impact of land use land cover changes on land surface temperature over Pune city, India. Quaternary International, vol. 575–576, 259–269. https://doi.org/10.1016/j.quaint.2020.04.052.

Gule T.T., Lemma B., Hailu B.T. (2023). Implications of land use/land cover dynamics on urban water quality: Case of Addis Ababa city, Ethiopia. Heliyon, 9(5). https://doi.org/10.1016/j.heliyon.2023.e15665.

Hagos M., Koeberl C., Van Wyk De Vries B. (2016a). The Quaternary volcanic rocks of the northern Afar Depression (northern Ethiopia): Perspectives on petrology, geochemistry, and tectonics. Journal of African Earth Sciences, 117, 29–47. https://doi.org/10.1016/j.jafrearsci.2015.11.022.

Hagos M., Koeberl C., Van Wyk De Vries B. (2016b). The Quaternary volcanic rocks of the northern Afar Depression (northern Ethiopia): Perspectives on petrology, geochemistry, and tectonics. Journal of African Earth Sciences, 117, 29–47. https://doi.org/10.1016/j.jafrearsci.2015.11.022.

Imran H.M., Hossainm A., Shammas M.I., Das M.K., Islam Md.R., Rahman K., Almazroui M. (2022). Land surface temperature and human thermal comfort responses to land use dynamics in Chittagong city of Bangladesh. Geomatics, Natural Hazards and Risk, 13(1), 2283–2312. https://doi.org/10.1080/19475705.2022.2114384.

Khovalyg D., Kazanci O.B., Halvorsen H., Gundlach I., Bahnfleth W.P., Toftum J., Olesen, B.W. (2020). Critical review of standards for indoor thermal environment and air quality. Energy and Buildings, 213,. https://doi.org/10.1016/j.enbuild.2020.109819.

Lin Y.C., Jung C.R., Hwang B.F., Chen C.P. (2025). Investigating wet-bulb globe temperature on heat-related illness in general population for alerting heat exposure: A time-stratified case-crossover study. Urban Climate, 59. https://doi.org/10.1016/j.uclim.2025.102322.

Liu Z., Li Z., Zeng Z., Luo M., Zhu R., Wang Y. (2026). Real-time sensing of hourly human thermal comfort by integrating AI, satellite images, and ground observations. Remote Sensing Applications: Society and Environment. https://doi.org/10.1016/j.rsase.2026.102042.

Mansourmoghaddam M., Rousta I., Ghafarian Malamiri H.R. (2022). Evaluation of the classification accuracy of NDVI index in the preparation of land cover map. Desert, 27(2). https://doi.org/10.22059/jdesert.2022.90834.

Matković F., Brajša R., Kuhar M., Benz A.O., Ludwig H.G., Selhorst C.L., Skokić I., Sudar D., Hanslmeier A. (2024). Calculated brightness temperatures of solar structures compared with ALMA and Metsähovi measurements. Astronomische Nachrichten, 345(5). https://doi.org/10.1002/asna.20230149.

Matthew M.W., Adler-Golden S.M., Berk A., Felde G., Anderson G.P., Gorodetzky D., Paswaters S., Shippert M. (2002). Atmospheric correction of spectral imagery: Evaluation of the FLAASH algorithm with AVIRIS data. Applied Imagery Pattern Recognition Workshop, 2002. Proceedings, 157–163. https://doi.org/10.1109/AIPR.2002.1182270.

Mohammadian F., Sahl Abadi A. S., Giahi O., Khoubi J., Zarei A.A., Boghsani G.T., Abbaspour S. (2019). Evaluation of Occupational Exposure to Heat Stress and Physiological Responses of Workers in the Rolling Industry. The Open Public Health Journal, 12(1), 114–120. https://doi.org/10.2174/1874944501912010114.

Morakinyo T.E., Ishola K.A., Eresanya E.O., Daramola M.T., Balogun I.A. (2024). Spatio-temporal characteristics of Heat stress over Nigeria using evaluated ERA5-HEAT reanalysis data. Weather and Climate Extremes, 45. https://doi.org/10.1016/j.wace.2024.100704.

Mustafa E.K., Co Y., Liu G., Kaloop M.R., Beshr A.A., Zarzoura F., Sadek M. (2020). Study for Predicting Land Surface Temperature (LST) Using Landsat Data: A Comparison of Four Algorithms. Advances in Civil Engineering, 2020, 1–16. https://doi.org/10.1155/2020/7363546.

Nam C., Lierhammer L., Buntemeyer L., Evadzi P., Cabana D., Celliers L. (2024). Changes in universal thermal climate index from regional climate model projections over European beaches. Climate Services, 34. https://doi.org/10.1016/j.cliser.2024.100447.

Neinavaz E., Skidmore A.K., Darvishzadeh R. (2020). Effects of prediction accuracy of the proportion of vegetation cover on land surface emissivity and temperature using the NDVI threshold method. International Journal of Applied Earth Observation and Geoinformation, 85. https://doi.org/10.1016/j.jag.2019.101984.

Şahin M.T., Hadimli H., Çakır Ç., Yasak Ü., Genişyürek F. (2025). The Role of Urban Landscape on Land Surface Temperature: The Case of Muratpaşa, Antalya. Land, 14(4), 663. https://doi.org/10.3390/land14040663.

Sen J., Nag P.K. (2019). Effectiveness of human-thermal indices: Spatio–temporal trend of human warmth in tropical India. Urban Climate, 27, 351–371. https://doi.org/10.1016/j.uclim.2018.11.009.

Shen H., Jiang Y., Li T., Cheng Q., Zeng C., Zhang L. (2020). Deep learning-based air temperature mapping by fusing remote sensing, station, simulation and socioeconomic data. Remote Sensing of Environment, 240, 1. https://doi.org/10.1016/j.rse.2020.111692.

Sim W.D., Yim J.S., Lee J.S. (2024). Assessing Land Cover Classification Accuracy: Variations in Dataset Combinations and Deep Learning Models. Remote Sensing, 16(14). https://doi.org/10.3390/rs16142623.

Steeneveld G.J., Koopmans S., Heusinkveld B.G., Van Hove L.W.A., Holtslag A.A.M. (2011). Quantifying urban heat island effects and human comfort for cities of variable size and urban morphology in the Netherlands. Journal of Geophysical Research, 116(D20). https://doi.org/10.1029/2011JD015988.

Stroppiana D., Bordogna G., Carrara P., Boschetti M., Boschetti L., Brivio P.A. (2012). A method for extracting burned areas from Landsat TM/ETM+ images by soft aggregation of multiple Spectral Indices and a region growing algorithm. ISPRS Journal of Photogrammetry and Remote Sensing, 69, 88–102. https://doi.org/10.1016/j.isprsjprs.2012.03.001.

Tan J., Yu D., Li Q., Tan X., Zhou W. (2020). Spatial relationship between land-use/land-cover change and land surface temperature in the Dongting Lake area, China. Scientific Reports, 10(1), 9245. https://doi.org/10.1038/s41598-020-66168-6.

Thom E.C. (1959). The Discomfort Index. Weatherwise, 12(2), 57–61. https://doi.org/10.1080/00431672.1959.9926960.

Thornton P.K., Van De Steeg J., Notenbaert A., Herrero M. (2009). The impacts of climate change on livestock and livestock systems in developing countries: A review of what we know and what we need to know. Agricultural Systems, 101(3), 113–127. https://doi.org/10.1016/j.agsy.2009.05.002.

Ullah W., Ahmad K., Ullah S., Tahir A.A., Javed M.F., Nazir A., Abbasi A.M., Aziz M., Mohamed A. (2023). Analysis of the relationship among land surface temperature (LST), land use land cover (LULC), and normalized difference vegetation index (NDVI) with topographic elements in the lower Himalayan region. Heliyon, 9(2). https://doi.org/10.1016/j.heliyon.2023.e13322.

Wei B., Bao Y., Yu S., Yin S., Zhang Y. (2021). Analysis of land surface temperature variation based on MODIS data a case study of the agricultural pastural ecotone of northern China. International Journal of Applied Earth Observation and Geoinformation, 100. https://doi.org/10.1016/j.jag.2021.102342.

Xu H., Hu X., Guan H., He G. (2017). Development of a fine-scale discomfort index map and its application in measuring living environments using remotely-sensed thermal infrared imagery. Energy and Buildings, 150, 598–607. https://doi.org/10.1016/j.enbuild.2017.06.003.

Yeo L.B., Ling G.H.T., Tan M.L., Leng P.C. (2021). Interrelationships between Land Use Land Cover (LULC) and Human Thermal Comfort (HTC): A Comparative Analysis of Different Spatial Settings. Sustainability, 13(1), 382. https://doi.org/10.3390/su13010382.

Zare S., Hasheminejad N., Bateni M., Baneshi M.R., Shirvan H.E., Hemmatjo R. (2020). The association between wet-bulb globe temperature and other thermal indices (DI, MDI, PMV, PPD, PHS, PSI and PSI_{hr}): A field study. International Journal of Occupational Safety and Ergonomics, 26(1), 71–79. https://doi.org/10.1080/10803548.2018.1475957.

Zare S., Hasheminejad N., Shirvan H.E., Hemmatjo R., Sarebanzadeh K., Ahmadi S. (2018). Comparing Universal Thermal Climate Index (UTCI) with selected thermal indices/environmental parameters during 12 months of the year. Weather and Climate Extremes, 19, 49–57. https://doi.org/10.1016/j.wace.2018.01.004.

Zhang H., Qi Z., Ye X., Cai Y., Ma W., Chen M. (2013). Analysis of land use/land cover change, population shift, and their effects on spatiotemporal patterns of urban heat islands in metropolitan Shanghai, China. Applied Geography, 44, 121–133. https://doi.org/10.1016/j.apgeog.2013.07.021.